International Journal on Advances in Telecommunications, vol 4 no 1 & 2, year 2011, http://www.iariajournals.org/telecommunications/

Capacity Analysis and Simulation of 3-D Space-Time Correlated HAP-MIMO Channels

Emmanouel T. Michailidis and Athanasios G. Kanatas
Department of Digital Systems
University of Piraeus
Piraeus, Greece
{emichail, kanatas}@unipi.gr

***Abstract*—High-altitude platforms (HAPs) are one of the most promising alternative infrastructures for realizing next generation mobile communications networks. This paper utilizes a recently proposed three-dimensional (3-D) reference multiple-input multiple-output (MIMO) channel model for HAPs and investigates the capacity of spatially and temporally correlated HAP-MIMO channels. The effect of several parameters, such as the elevation angle of the platform, the configuration and displacement of the antenna arrays, the Doppler spread, and the 3-D non-uniform distribution of the local scatterers, on the capacity is studied. Based on the reference model, a 3-D sum-of-sinusoids (SoS) deterministic simulation model for HAP-MIMO channels is proposed. The results show that the simulation model is a good approximation of the reference model.**

Keywords-Capacity; 3-D scattering model; correlation; high-altitude platform (HAP); multiple-input multiple-output (MIMO) channel; Ricean fading; simulation

I. INTRODUCTION

Wireless communications services are traditionally provided by terrestrial and satellite systems. Terrestrial links are widely used to provide services in areas with complex propagation conditions, while satellite links are usually used to provide high-speed connections, where terrestrial infrastructure is not available. These systems represent two well established infrastructures that have been dominant in the telecommunications arena for years. Recently, an alternative wireless communications technology has emerged known as high-altitude platforms (HAPs) and has attracted considerable attention worldwide [1]-[6]. The term HAPs defines aerial platforms flying at an altitude of approximately 20 km above the ground, in the stratosphere. Among the frequency bands that the International Telecommunication Union (ITU) has licensed for communications through HAPs is the 2 GHz frequency band for mobile communications services [7].

The growing exigencies for spectral efficiency and higher data-rates have prompted the development of advanced physical layer techniques. Hence, it is crucial we apply and/or originate techniques in order to construct high-performance HAP-based systems. At these measures, the multiple-input multiple-output (MIMO) technology is a potential candidate, since it can significantly upgrade the performance of wireless communications networks and surpass the conventional single-input single-output (SISO) technology [8]-[11]. The performance of MIMO systems strongly depends on the channel characteristics, which are mainly determined by the antenna configuration and the richness of scattering. Therefore, the signals coming from HAPs to terrestrial stations are affected by the physical environment and the geometrical characteristics of the link.

Recently, the authors proposed a three-dimensional (3-D) geometry-based model for HAP-MIMO channels and justified its geometry [2]. In this paper, which is an extended and thorough version of [1], the reference model is utilized to analytically study the capacity of HAP-MIMO channels. Several parameters are considered, e.g., the elevation angle of the platform, the array configuration, the Doppler spread, and the 3-D non-isotropic distribution of the scatterers. The impact of each parameter on the capacity is separately examined and extensive numerical results are provided. The stratospheric winds may cause variations in the position of the platform [12][13]. Hence, this paper extends [1] and goes further to investigate the influence of any possible displacement of the HAP antennas on the channel capacity.

To the best of the authors' knowledge, there are no experimental data available in the literature to verify the theoretical results. However, simulation of fading channels in software is commonly used as opposed to field trials, because it allows for cost-effective and time-saving system analysis, design, test, and verification. The prime requirement of a simulation set-up is to capture the fading effects created by the radio channel and the goal of any simulation model is to properly reproduce the channel properties. Many different methods have been adopted for the simulation of fading channels. Among them, the sum-of-sinusoids (SoS) principle introduced by Rice [14] has been widely accepted by academia and industry as an adequate basis for the design of simulation models for cellular channels [15]-[17]. According to this principle, the overall channel waveform is the sum of several complex sinusoids having frequencies, amplitudes and phases that are appropriately selected to accurately approximate the desired statistical properties. Indeed, the complexity of the SoS-based models is typically reduced by cleverly choosing the model parameters to reduce the computation load. Furthermore, SoS-based models can be easily extended to develop simulation channel models for MIMO systems due to their explicit inclusion of spatial information, e.g., the multipath angles of arrival and departure.

Owing to these advantages, this paper proposes a 3-D deterministic SoS-based simulation model for HAP-MIMO channels. The deterministic models are easy to implement and have short simulation times. Specifically, they have fixed parameters for all simulation trials and converge to the desired properties in a single simulation trial leading to deterministic statistical properties [16]. The simulation results demonstrate the usefulness of the proposed simulation model.

The rest of the paper is organized as follows. Section II briefly reviews the 3-D reference model, while Section III describes the channel statistics. Section IV studies the HAP-MIMO channel capacity and provides numerical results. Section V details the deterministic simulation model and provides simulation results. Finally, concluding remarks are drawn in Section VI.

II. THE 3-D REFERENCE MODEL

This paper considers a downlink HAP-MIMO communication channel with n_T transmit and n_R receive omni-directional antenna elements at a quasi-stationary Stratospheric Base Station (SBS) and a Terrestrial Mobile Station (TMS), respectively. The antennas are numbered as $1 \le p \le q \le n_T$ and $1 \le l \le m \le n_R$, respectively. Frequencies well below 10 GHz are utilized. Hence, both line-of-sight (LoS) and non-line-of-sight (NLoS) links are considered, while rain effects are insignificant.

The geometrical characteristics of the reference model and the definition of the Cartesian coordinate system are discussed in Figures 1 and 2. Figure 1 shows the 3-D model for a 2×2 HAP-MIMO channel, while Figure 2 presents the projection of this model to the *x*-*y* plane. Based on this simple configuration, uniform linear arrays (ULAs) with an arbitrary number of antennas can be constructed. The *x*-axis is the line that connects coordinate origin O (centre of the projections of the SBS antenna elements to the *x*-*y* plane) and O' (lower center of the cylinder), while O_T and O_R represent the centers of the SBS and TMS arrays, respectively. The elevation angle of SBS relative to O_R is β_T and the heights of the SBS and TMS arrays are H_T and H_R, respectively. Then, the distance between O and O' is $D \approx H_T / \tan\beta_T$. The spacing between two adjacent antenna elements at the SBS and TMS is denoted by δ_T and δ_R, respectively, while α_{LoS}^{Rl} denotes the azimuth angle of arrival (AAoA) of the LoS paths. The angles θ_T and θ_R represent the orientation of the SBS and TMS antenna arrays respectively, and the angle ψ_R describes the elevation angle of the l^{th} TMS antenna element. Moreover, TMS is moving with speed v_R in the direction determined by the angle γ_R. It is assumed that $N \to \infty$ scatterers in the vicinity of the TMS are non-uniformly distributed within a cylinder of radius $R_{S,\max}$ and height $H_{S,\max}$ [2]. Then, the n^{th} scatterer is denoted by $S^{(n)}$, the distance between its projection to the *x*-*y* plane and O' is $R_S^{(n)} \in \left(0, R_{S,\max}\right]$, and its height is $H_S^{(n)} \in \left(0, H_{S,\max}\right]$. Finally, $\alpha_T^{(n)}$ and $\alpha_R^{(n)}$ denote the azimuth angle of departure (AAoD) of the waves that impinge on $S^{(n)}$ and the AAoA of the waves scattered from $S^{(n)}$, respectively.

The displacement due to the winds or pressure variations of the stratosphere is a major problem to be faced [12], [13]. In practice, there are 6 degrees of freedom to which HAPs are subjected. Specifically, HAPs may be displaced in any direction at a varying speed, and the displacements can be shifting along the *x*-, *y*-, and *z*-axes, as well as roll, pitch, and yaw. Considering that SBS antenna elements are installed along the SBS, rotation with respect to the *x*-axis corresponds to pitch, rotation on the *y*-axis corresponds to roll and rotation along *z*-axis corresponds to yaw (see Figure 1). Note that pitch corresponds to an elevation of the p^{th} SBS antenna element, which is described by the angle ψ_T. For ease of reference, the parameters of the reference model are summarized in Table I.

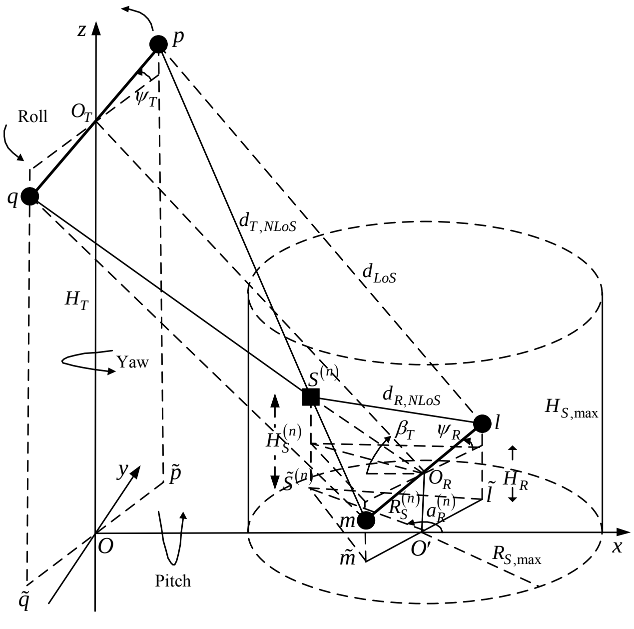

Figure 1. LoS and NLoS paths of the 3-D model for a 2×2 HAP-MIMO channel.

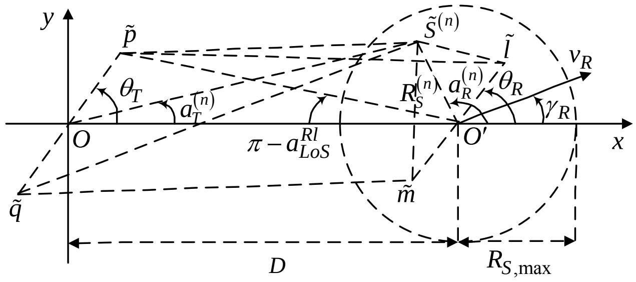

Figure 2. LoS and NLoS paths of the projection of the 3-D model to the x-y plane for a 2×2 HAP-MIMO channel.

TABLE I
DEFINITION OF THE MODEL PARAMETERS

D	The distance between the centre O of the projections of the SBS antenna elements to the x-y plane and the lower centre O' of the cylinder.
$R_{S,\max}$, $H_{S,\max}$	The radius and the height of the cylinder with the scatterers, respectively.
δ_T, δ_R	The spacing between two adjacent antenna elements at the SBS and TMS, respectively.
θ_T, θ_R	The orientation of the SBS and TMS antennas in the x-y plane (relative to the x-axis), respectively.
ψ_T, ψ_R	The elevation angle of the l^{th} TMS antenna element and the p^{th} SBS antenna element, respectively, relative to the x-y plane.
v_R	The velocity of the TMS.
γ_R	The moving direction of the TMS.
β_T	The elevation angle of the SBS relative to O_R.
H_T, H_R, $H_S^{(n)}$	The height of the SBS, the TMS, and the n^{th} scatterer, respectively.
a_{LoS}^{Rl}	The azimuth angle of arrival of the LoS paths.
$a_T^{(n)}$, $a_R^{(n)}$	The azimuth angle of arrival and the azimuth angle of departure at/from the n^{th} scatterer, respectively
$R_S^{(n)}$	The distance between O' and the projection of the n^{th} scatterer to the x-y plane.
$\varphi^{(n)}$	The random phase introduced by the n^{th} scatterer.
μ	The mean azimuth angle at which the scatterers are distributed in the x-y plane (von Mises distribution).
k	The spread of the scatterers around the mean azimuth angle (von Mises distribution).
a	The spread of the scatterers around the TMS (hyperbolic distribution).
$H_{S,\text{mean}}$	The mean of scatterer's height (log-normal distribution).
σ	The standard deviation of scatterer's height (log-normal distribution).

III. CHANNEL STATISTICS

A HAP-based communication channel is expected to be Ricean in its general form [3]. Hence, the impulse response $h_{pl}(t)$ of the sub-channel p-l is a superposition of the LoS and NLoS rays and is given by

$$h_{pl}(t) = \sqrt{\frac{K_{pl}}{K_{pl}+1}}\, h_{pl,LoS}(t) + \sqrt{\frac{1}{K_{pl}+1}}\, h_{pl,NLoS}(t), \quad (1)$$

where K_{pl} is the Ricean factor of the sub-channel p-l. The LoS and NLoS components of the impulse response, are expressed, respectively, as follows [2]

$$h_{pl,LoS}(t) = e^{-j\frac{2\pi}{\lambda} d_{LoS}}\, e^{-j2\pi t f_{R,\max}\cos\gamma_R}, \quad (2)$$

$$h_{pl,NLoS}(t) = \lim_{N\to\infty} \frac{1}{\sqrt{N}} \sum_{n=1}^{N} e^{-j\frac{2\pi}{\lambda}\left(d_{T,NLoS}+d_{R,NLoS}\right)}$$
$$\times e^{j\varphi^{(n)}}\, e^{j2\pi t f_{R,\max}\cos\left(a_R^{(n)}-\gamma_R\right)\cos\left[\arctan\left(H_S^{(n)}/R_S^{(n)}\right)\right]}, \quad (3)$$

where $f_{R,\max} = v_R/\lambda$ is the maximum Doppler frequency associated with TMS, λ is the carrier wavelength, and $\varphi^{(n)}$ is the random phase introduced by the n^{th} scatterer. Considering that $\left\{R_{S,\max}, \delta_T\right\} \ll D$, $\delta_R \ll R_{S,\max}$, and $H_T \gg \left\{H_R, H_{S,\max}\right\}$, one can show that the distances d_{LoS}, $d_{T,NLoS}$, and $d_{R,NLoS}$ can be approximated as [2]

$$d_{LoS} \approx \frac{D}{\cos\beta_T} - \frac{0.5\left(n_T+1-2p\right)\delta_T\cos\theta_T\cos\psi_T}{\cos\beta_T}$$
$$+\frac{0.5\left(n_R+1-2l\right)\delta_R\cos\theta_R\cos\psi_R}{\cos\beta_T}, \quad (4)$$

$$d_{T,NLoS} \approx \frac{D}{\cos\beta_T} - \frac{0.5\left(n_T+1-2p\right)\delta_T\cos\theta_T\cos\psi_T}{\cos\beta_T}$$
$$-\frac{0.5\left(n_T+1-2p\right)\delta_T\sin\theta_T\cos\psi_T R_S^{(n)}\sin a_R^{(n)}}{D\cos\beta_T}, (5)$$

$$d_{R,NLoS} \approx R^{(n)}/\cos\left[\arctan\left(H_S^{(n)}/R_S^{(n)}\right)\right] - 0.5\left(n_R+1-2l\right)$$
$$\times\delta_R\cos\psi_R\cos\left(\theta_R-\alpha_R^{(n)}\right)\cos\left[\arctan\left(H_S^{(n)}/R_S^{(n)}\right)\right]$$
$$-0.5\left(n_R+1-2l\right)\delta_R\sin\psi_R\sin\left[\arctan\left(H_S^{(n)}/R_S^{(n)}\right)\right]. \quad (6)$$

Since the number of local scatterers is infinite, central limit theorem implies that $h_{pl,NLoS}(t)$ is a lowpass zero-mean complex Gaussian process. Hence, the envelope $\left|h_{pl,NLoS}(t)\right|$ is Rayleigh distributed.

The space-time correlation function (STCF) between two arbitrary subchannels $h_{pl,NLoS}\left(t\right)$ and $h_{qm,NLoS}\left(t\right)$ is defined as

$$R_{pl,qm}^{NLoS}\left(\delta_T,\delta_R,\tau,t\right)=\mathrm{E}\left[h_{pl,NLoS}\left(t\right)h_{qm,NLoS}^{*}\left(t+\tau\right)\right], \quad (7)$$

where $\left(\cdot\right)^{*}$ denotes complex conjugate operation and $\mathrm{E}\left[\cdot\right]$ is the statistical expectation operator. The number of local scatterers in the reference model is infinite. Thus, the discrete variables $a_R^{(n)}$, $R_S^{(n)}$ and $H_S^{(n)}$ can be replaced with continuous random variables a_R, R_S and H_S with joint probability density function (pdf) $f\left(a_R,R_S,H_S\right)$. From Figure 1, the aforementioned variables are independent. Therefore, the joint pdf $f\left(a_R,R_S,H_S\right)$ can be decomposed to the product $f\left(a_R\right)f\left(R_S\right)f\left(H_S\right)$.

The experimentally verified von Mises pdf [18], [19] is used to characterize a_R and is defined as

$$f\left(a_R\right)=\frac{e^{k\cos\left(a_R-\mu\right)}}{2\pi I_0\left(k\right)},\ -\pi\le a_R\le\pi, \quad (8)$$

where $I_0\left(\cdot\right)$ is the zeroth-order modified Bessel function of the first kind, $\mu\in\left[-\pi,\pi\right]$ is the mean angle at which the scatterers are distributed in the *x*-*y* plane, and $k\ge 0$ controls the spread around μ. In addition, the experimentally verified hyperbolic pdf [20], [21] is used to characterize R_S and is defined as

$$f\left(R_S\right)=\frac{a}{\tanh\left(aR_{S,\max}\right)\cosh^2\left(aR_S\right)},\ 0<R_S\le R_{S,\max}, \quad (9)$$

where $a\in\left(0,1\right)$ controls the spread of the scatterers around the TMS. Moreover, the experimentally verified log-normal pdf [22], [23] is used to characterize H_S and is defined as

$$f\left(H_S\right)=\frac{e^{-\frac{1}{2\sigma^2}\ln^2\left(\frac{H_S}{H_{S,\mathrm{mean}}}\right)}}{H_S\sigma\sqrt{2\pi}},\ 0<H_S\le H_{S,\max}, \quad (10)$$

where $H_{S,\mathrm{mean}}$ and σ are the mean and standard deviation of H_S, respectively. Finally, using (3) and (5)-(10), and the equality $\int_{-\pi}^{\pi}e^{a\sin(c)+b\cos(c)}dc=2\pi I_0\left(\sqrt{a^2+b^2}\right)$ [24, eq.3.338-4], the STCF of the NLoS component is derived as follows

$$R_{pl,qm}^{NLoS}=\int_0^{H_{S,\max}}\int_0^{R_{S,\max}}x_1 I_0\left(\sqrt{x_2^2+x_3^2}\right)dR_S\,dH_S, \quad (11)$$

where

$$x_1=\frac{a\cdot e^{j\frac{2\pi(q-p)\delta_T\cos\theta_T\cos\psi_T}{\lambda\cos\beta_T}}}{\sigma\sqrt{2\pi}\tanh\left(aR_{S,\max}\right)I_0\left(k\right)}$$
$$\times\frac{e^{-\frac{1}{2\sigma^2}\ln^2\left(\frac{H_S}{H_{S,\mathrm{mean}}}\right)}e^{j\frac{2\pi(m-l)\delta_R\sin\psi_R\sin\left[\arctan\left(H_S/R_S\right)\right]}{\lambda}}}{H_S\cosh^2\left(aR_S\right)}, \quad (12)$$

$$x_2=j\frac{2\pi\left(q-p\right)\delta_T\sin\theta_T\cos\psi_T R_S}{\lambda D\cos\beta_T}$$
$$+j\frac{2\pi\left(m-l\right)\delta_R\sin\theta_R\cos\psi_R\cos\left[\arctan\left(H_S/R_S\right)\right]}{\lambda}$$
$$-j2\pi\tau f_{R,\max}\sin\gamma_R\cos\left[\arctan\left(H_S/R_S\right)\right]+k\sin\mu, \quad (13)$$

$$x_3=j\frac{2\pi\left(m-l\right)\delta_R\cos\theta_R\cos\psi_R}{\lambda}\cos\left[\arctan\left(H_S/R_S\right)\right]$$
$$-j2\pi\tau f_{R,\max}\cos\gamma_R\cos\left[\arctan\left(H_S/R_S\right)\right]+k\cos\mu. \quad (14)$$

The double integral in (11) has to be evaluated numerically, since there is no closed-form solution.

IV. CAPACITY ANALYSIS OF 3-D HAP-MIMO CHANNELS

In this section, the HAP-MIMO channel capacity is defined and the utility of the reference model is demonstrated. Numerical results are provided and the influence of the model parameters on the capacity is studied.

It is assumed that the channel is known to the TMS and unknown to the SBS. Then, the HAP-MIMO channel capacity can be obtained from [9]

$$C=\log_2\det\left(\mathbf{I}_{n_R}+\left(\frac{SNR}{n_T}\right)\mathbf{HH}^H\right)bps/Hz, \quad (15)$$

where $\mathbf{H}$ is the $n_R\times n_T$ channel matrix, $\mathbf{I}_{n_R}$ is an identity matrix of size n_R, SNR corresponds to the average receive signal-to-noise ratio, $\left(\cdot\right)^H$ denotes the complex conjugate (Hermitian) transpose operator, and $\det\left(\cdot\right)$ denotes the matrix determinant. Throughout this paper, the notion of ergodic capacity is also employed, which corresponds to the expectation of the instantaneous channel capacity

$$C_{erg}=\mathrm{E}\left[\log_2\det\left(\mathbf{I}_{n_R}+\left(\frac{\mathrm{SNR}}{n_T}\right)\mathbf{HH}^H\right)\right]\ \mathrm{bps/Hz}. \quad (16)$$

Since the channel is Ricean in general, $\mathbf{H}$ is given by

$$\mathbf{H}=\sqrt{\frac{K}{K+1}}\mathbf{H}_{LoS}+\sqrt{\frac{1}{K+1}}\mathbf{H}_{NLoS}, \quad (17)$$

where $\mathbf{H}_{LoS}$ is the $n_R \times n_T$ matrix containing the LoS responses among the antenna elements, $\mathbf{H}_{NLoS}$ is the $n_R \times n_T$ matrix containing the NLoS responses due to the scattered waves and K is the Ricean factor.

The elements of $\mathbf{H}_{LoS}$ can be obtained using (2) and (4) as follows

$$\mathbf{H}_{LoS} = \begin{bmatrix} h_{11,LoS} & \cdots & h_{1n_T,LoS} \\ \vdots & \ddots & \vdots \\ h_{n_R1,LoS} & \cdots & h_{n_Rn_T,LoS} \end{bmatrix}. \qquad (18)$$

The matrix $\mathbf{H}_{NLoS}$ can be evaluated after a large number of channel realizations using the following equation [25]

$$\mathrm{vec}(\mathbf{H}_{NLoS}) = \mathbf{R}_{NLoS}^{1/2}\mathrm{vec}(\mathbf{H}_w), \qquad (19)$$

where $\mathbf{R}_{NLoS}$ is the $n_Rn_T \times n_Rn_T$ correlation matrix associated with the NLoS component, $\mathbf{R}_{NLoS}^{1/2}$ is the square root of $\mathbf{R}_{NLoS}$ that satisfies $\mathbf{R}_{NLoS}^{1/2}\mathbf{R}_{NLoS}^{H/2} = \mathbf{R}_{NLoS}$, $\mathbf{H}_w$ is a $n_R \times n_T$ stochastic matrix with independent and identically distributed (i.i.d.) zero mean complex Gaussian entries, and $\mathrm{vec}(\cdot)$ denotes matrix vectorization[1]. Using (11)-(14), $\mathbf{R}_{NLoS}$ is given by

$$\mathbf{R}_{NLoS} = \begin{bmatrix} R_{11,11}^{NLoS} & R_{11,21}^{NLoS} & \cdots & R_{11,n_Rn_T}^{NLoS} \\ R_{21,11}^{NLoS} & \ddots & & R_{21,n_Rn_T}^{NLoS} \\ \vdots & & \ddots & \vdots \\ R_{n_Rn_T,11}^{NLoS} & \cdots & & R_{n_Rn_T,n_Rn_T}^{NLoS} \end{bmatrix}. \qquad (20)$$

Finally, the channel matrix is normalized so that the constraint

$$\mathrm{E}\left[\|\mathbf{H}\|_\mathrm{F}^2\right] = n_T n_R \qquad (21)$$

is fulfilled, where $\|\cdot\|_\mathrm{F}$ represents the Frobenius norm of a matrix. This normalization corresponds to a system with perfect power control [26] and makes SNR independent of $\mathbf{H}$.

A. Numerical Results

This subsection investigates the effect of the model parameters on the capacity of space-time correlated HAP-MIMO channels. These parameters control the correlation between the subchannels [2]. In particular, the correlation depends on the degree of scattering in a specific propagation environment and the antenna inter-element spacing at both the transmitter and the receiver. Hence, dense scattering in the propagation environment in combination with adequate antenna spacing ensure decorrelation. Considering coherent diffuse components or sparse scattering and increased correlation, the rank of the channel matrix is deficient and the spectral efficiency is low. Therefore, the model parameters control the performance issues, i.e., the spatial multiplexing gain and the capacity enhancement. Unless indicated otherwise, the values of the model parameters used to obtain the curves are $H_T = 20$ km, $\beta_T = 60^\circ$, $\delta_T = 50\lambda$, $\delta_R = 0.5\lambda$, $\theta_T = \theta_R = 90^\circ$, $\psi_T = \psi_R = 0^\circ$, $k = 3$, $\mu = 0^\circ$, $a = 0.01$ (this value corresponds to a mean R_S of about 60 m [2]), $R_{S,\max} = 200$ m, $H_{S,\max} = 70$ m, $f_{R,\max} = 100$ Hz, $\gamma_R = 60^\circ$, $\mathrm{SNR} = 18$ dB, and $K_{pl} = K_{qm} = K = 3$ dB. A typical densely built-up district (London, U.K. [22]) is considered and we set $H_{S,\mathrm{mean}} = 17.6$ m and $\sigma = 0.31$, i.e., the surrounding buildings act as scatterers. Finally, a normalized Doppler frequency $f_n = f_{R,\max}T_s = 0.01$ is used, where T_s is the sampling period.

Figures 3 and 4 compare the ergodic capacity obtained using a HAP-MIMO, i.e., $n_T = n_R = 2$, and a HAP-SISO, i.e., $n_T = n_R = 1$, architecture by varying the Ricean factor and the received SNR. One observes that maximum capacity is obtained in an ideal HAP-MIMO Rayleigh channel scenario. Then, the capacity increases up to 10.6 bps/Hz compared to the capacity of a HAP-SISO channel. However, the potential MIMO gain drastically degrades with the strength of the LoS component, i.e., increasing the Ricean factor increases the correlation and decreases the capacity gain. Providing that the propagation conditions are characterized by rich multipath, e.g., in dense urban areas, the benefits of MIMO technology can be even more obvious. On the contrary, HAP-SISO channels take advantage of the existence of a strong LoS signal, i.e., increasing the Ricean factor drastically increases the capacity. Note that the difference in capacity between HAP-MIMO and HAP-SISO architectures increases, as the SNR increases. However, this difference is nullified, when the SNR is low. Then, the rank of the channel matrix plays an important role. In addition, the channel capacity achieved using both architectures is invariable for $K > 10$ dB.

Figures 5-9 investigate the effect of spatial correlation on the channel capacity. Figure 5 shows the ergodic capacity as a function of the spacing δ_T between SBS antenna elements for different SBS elevation angle β_T and $K = 0$. One observes that increasing δ_T beyond approximately 70λ, 50λ, and 30λ, when $\beta_T = 50^\circ$, $\beta_T = 60^\circ$ and $\beta_T = 70^\circ$, respectively, has a negligible effect on the channel

---

[1] The vectorization of a matrix is a linear transformation, which converts the matrix into a column vector. Specifically, the vectorization of a $m \times n$ matrix A, denoted by $\mathrm{vec}(A)$, is the $mn \times 1$ column vector obtained by stacking the columns of the matrix A on top of one another.

capacity. According to [3], [4], HAPs are either airships (up to 200 m in length) or aircrafts (up to 30 m in length). Considering 2.1 GHz carrier frequency [7], the wavelength is equal to approximately 0.14 m. Hence, Figure 5 implies that applying MIMO techniques to a single HAP offers considerable capacity gain, as soon as the Ricean is small.

Figure 6 depicts the complementary cumulative distribution function (CCDF) of the capacity and examines the effect of SBS antenna array orientation on the capacity. One observes that SBS broadside antenna arrays, i.e., $\theta_T = 90^\circ$, provide maximum capacity. Moreover, decreasing θ_T from 90° to 60° has a negligible effect on the capacity. However, further decrease of θ_T significantly decreases the capacity. The capacity also depends on the relative angle between the TMS antenna array and the local scatterers around the TMS, i.e., θ_R-μ, and is maximized when the difference between θ_R and μ is 90° [17].

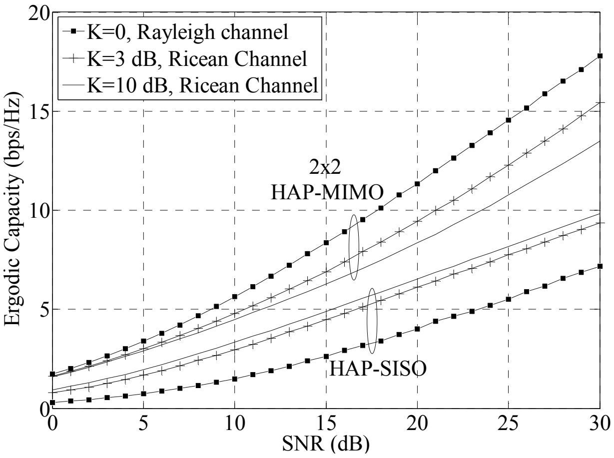

Figure 3. Comparison of the ergodic capacity obtained using the HAP-MIMO and HAP-SISO architectures as a function of the received SNR for different Ricean factor.

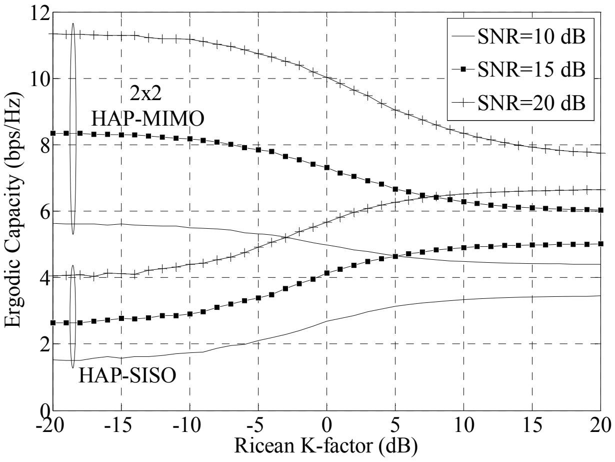

Figure 4. Comparison of the ergodic capacity obtained using the HAP-MIMO and HAP-SISO architectures as a function of the Ricean factor for different received SNR.

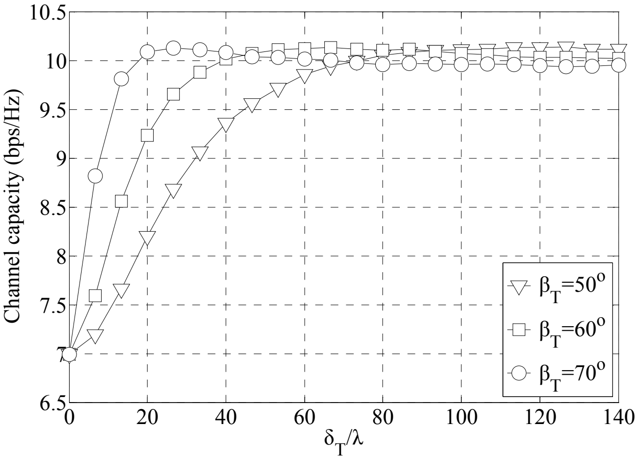

Figure 5. The ergodic capacity of a HAP-MIMO channel in terms of the spacing between the SBS antenna elements for different SBS elevation angle.

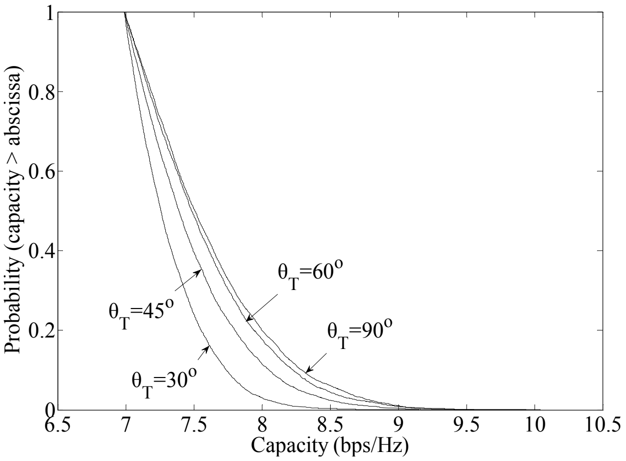

Figure 6. Contrasting complementary cumulative distribution function of the capacity of a HAP-MIMO channel for different antenna array orientation at the SBS.

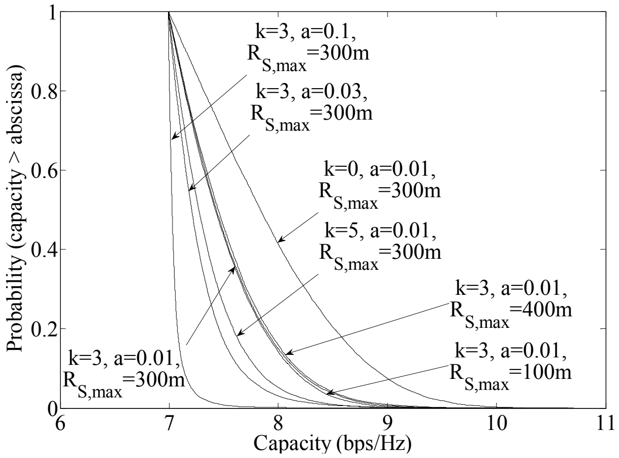

Figure 7. Contrasting complementary cumulative distribution function of the capacity of a HAP-MIMO channel for different degree of scattering, spread of scatterers, and maximum distance between TMS-scatterers.

Figure 7 depicts depicts the CCDF of the capacity and examines the influence of the parameters k, a, and $R_{S,\max}$ on the capacity, i.e., the influence of two-dimensional (2-D) scattering. The effect of each parameter is examined independently (keeping all other parameters fixed). Note that as k increases, the scattering becomes increasingly non-isotropic and the capacity decreases (due to the increase in spatial correlation [2]). Moreover, increasing a decreases the spread of scatterers and decreases the capacity (due to the increase in spatial correlation [2]). However, changing $R_{S,\max}$ has a negligible effect on the capacity and the spatial correlation [2].

Figure 8 shows the CCDF of the capacity, when the TMS antenna array is horizontally, i.e., $\psi_R = 0^\circ$, or vertically placed, i.e., $\psi_R = 90^\circ$, for different $H_{S,\text{mean}}$. Note that changing $H_{S,\text{mean}}$ has an insignificant influence on the capacity, when the TMS antenna array is horizontally placed. However, the capacity depends on the degree of urbanization, i.e., the heights of the scatterers, when the TMS antenna array is vertically placed. Then, increasing $H_{S,\text{mean}}$ increases the capacity. The difference between capacities of systems with horizontally and vertically placed TMS antenna array is nullified in highly urbanized areas. Figure 8 suggests that if the available area in the *x-y* plane is limited for antenna array realization, the TMS antenna array can be tilted without significant loss of capacity.

Figure 9 examines the effect of the temporal correlation by separately varying the normalized Doppler frequency f_n and the moving direction γ_R of the TMS. Observe that an increase in f_n results in an increase in channel capacity due to the decrease in temporal correlation. Furthermore, as γ_R increases (up to 180°), the TMS moves toward the SBS and the channel capacity increases.

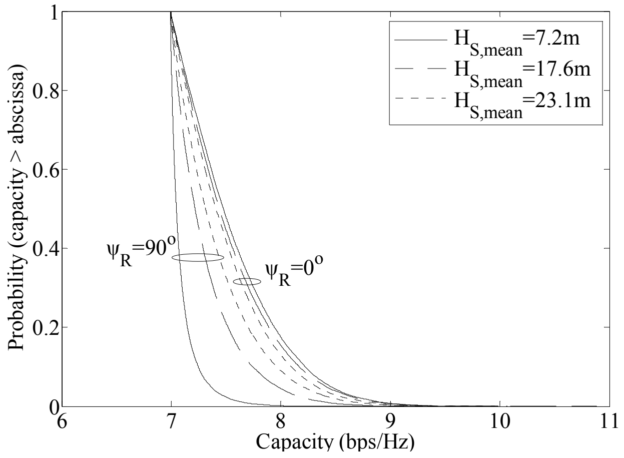

Figure 8. Contrasting complementary cumulative distribution function of the capacity of a HAP-MIMO channel for horizontally or vertically placed TMS antennas and different mean of the scatterer height.

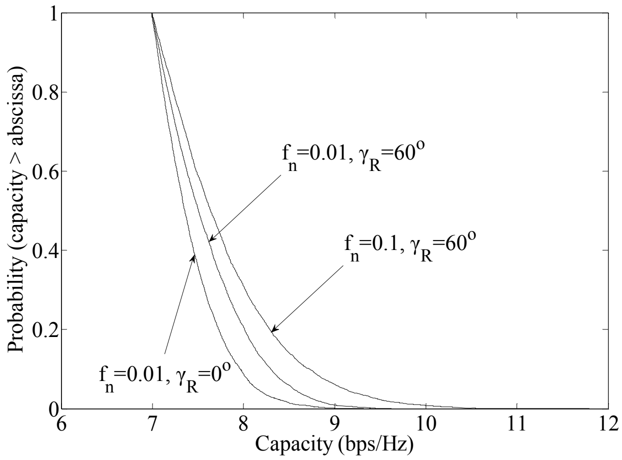

Figure 9. Contrasting complementary cumulative distribution function of the capacity of a HAP-MIMO channel for different normalized Doppler frequency and different moving direction at the TMS.

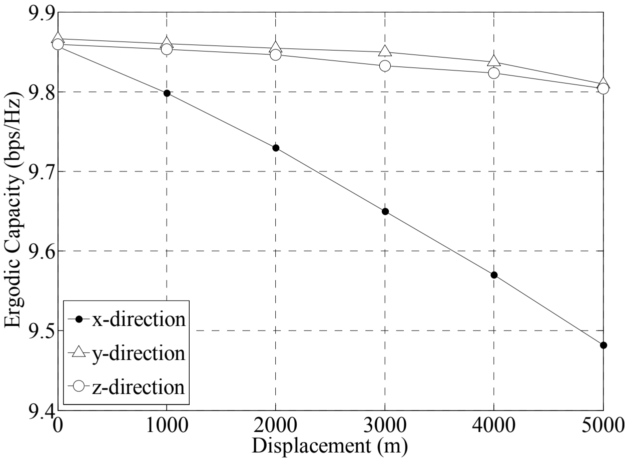

Figure 10. The ergodic capacity of a HAP-MIMO channel for different directions of SBS antenna displacement due to the stratospheric winds.

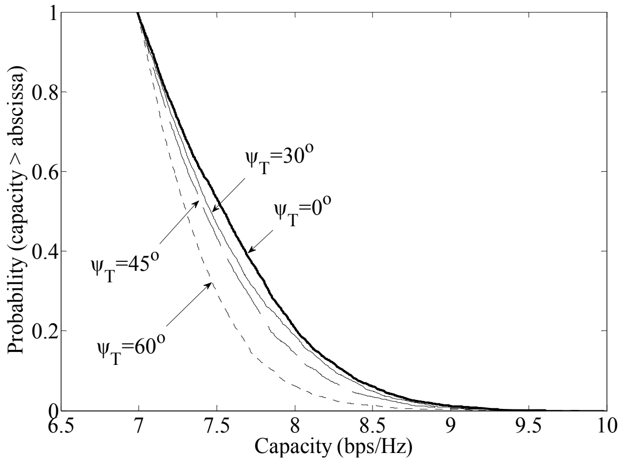

Figure 11. Contrasting complementary cumulative distribution function of the capacity of a HAP-MIMO channel for different elevation angle of the p^{th} SBS antenna element (pitch effect).

Figures 10 and 11 investigate the effect of HAP antenna displacement due to the stratospheric winds on the capacity of HAP-MIMO channels. The influence of each degree of freedom on the capacity is examined independently (keeping all other parameters fixed) in the following figures. Roll and pitch can be considered identical to each other, since both are based on similar principles. In addition, yaw corresponds to a change in the orientation of the SBS antenna array, which is described by the angle θ_T Therefore, Figure 6 represents also the yaw effect and the effect of only pitch and yaw on the capacity is studied.

Figure 10 demonstrates the influence of up to 5 km shifting along either x-, y- or z-axis on the capacity. One observes that the capacity is relatively insensitive to displacements along y- and z-axis. However, the capacity fairly decreases up to 0.5 bps/Hz or 4%, when the displacement takes place along x-axis.

Figure 11 depicts the effect of pitch on the capacity. Note that increasing ψ_T from 0° to 45° has a negligible effect on the capacity. However, further increase in ψ_T drastically decreases the capacity.

V. SIMULATION OF 3-D HAP-MIMO CHANNELS

The reference model assumes an infinite number of scatterers and prevents practical implementation. Hence, simulation models with finite number of scatterers are desirable. Under the framework of the reference model, a stochastic simulation model can be directly obtained by using a finite number N of scatterers. Then, considering a Ricean HAP-MIMO channel, the impulse response of the sub-channel p-l associated with the stochastic simulation model is given by

$$\hat{h}_{pl}(t)=\sqrt{\frac{K_{pl}}{K_{pl}+1}}h_{pl,LoS}(t)+\sqrt{\frac{1}{K_{pl}+1}}\hat{h}_{pl,NLoS}(t), \quad (22)$$

where

$$\hat{h}_{pl,NLoS}(t)=\frac{1}{\sqrt{N}}\sum_{n=1}^{N}e^{-j\frac{2\pi}{\lambda}\left(d_{T,NLoS}+d_{R,NLoS}\right)}e^{j\varphi^{(n)}}$$
$$\times e^{j2\pi t f_{R,\max}\cos\left(a_R^{(n)}-\gamma_R\right)\cos\left[\arctan\left(H_S^{(n)}/R_S^{(n)}\right)\right]} \quad (23)$$

is the NLoS component of the impulse response, $h_{pl,LoS}(t)$ is defined in (2), "$\hat{\cdot}$" describes a stochastic process, and $d_{T,NLoS}$ and $d_{R,NLoS}$ are defined in (5) and (6), respectively. The random variables $a_R^{(n)}$, $R_S^{(n)}$, and $H_S^{(n)}$ can be generated utilizing the distributions defined in Section II, while $\varphi^{(n)}$ is generated as a random variable uniformly distributed in the interval $[-\pi,\pi)$. All other parameters of the simulation model are identical with those of the reference model. Specifically, $a_R^{(n)}$ is modeled using the von Mises pdf and can be generated as

$$a_R^{(n)}=F_{a_R}^{-1}(\delta), \quad (24)$$

where δ is a random variable uniformly distributed in the interval $(0,1)$. The function $F_{a_R}^{-1}(\cdot)$ denotes the inverse function of the von Mises cumulative distribution function (cdf) and can be evaluated using the numerical method presented in [27]. In addition, $R_S^{(n)}$ is modeled using the hyperbolic pdf and can be generated as

$$R_S^{(n)}=F_{R_S}^{-1}(\zeta), \quad (25)$$

where ζ is a random variable uniformly distributed in the interval $(0,1)$. The function $F_{R_S}(\cdot)$ denotes the hyperbolic cdf, which is given by

$$F_{R_S}(R_S)=\tanh(aR_S)/\tanh(aR_{S,\max}). \quad (26)$$

Finally, $H_S^{(n)}$ is modeled using the log-normal pdf and can be generated as

$$H_S^{(n)}=F_{H_S}^{-1}(\xi), \quad (27)$$

where ξ is a random variable uniformly distributed in the interval (0,1). The function $F_{H_S}(\cdot)$ denotes the log-normal cdf, which is given by

$$F_{H_S}(H_S)=\frac{1}{2}\mathrm{erfc}\left[-\frac{\ln(H_S)-\ln(H_{S,\mathrm{mean}})}{\sigma\sqrt{2}}\right], \quad (28)$$

where $\mathrm{erfc}(x)=\left(2/\sqrt{\pi}\right)\int_x^{\infty}e^{-u^2}du$ is the complementary error function.

To simulate a HAP-MIMO channel, this generic stochastic simulation model can be directly applied by generating the variables $a_R^{(n)}$, $R_S^{(n)}$, $H_S^{(n)}$, and $\varphi^{(n)}$. However, due to the high degree of randomness during the computation of these variables, an infinite number of simulation trials is required and the stochastic simulation model is still non-realizable and inefficient. Hence, one must otherwise determine the model parameters, in order to fully exploit the inherent advantages of the SoS principle. This procedure is called the parameter computation method and the type of a simulation model is directly related to this method.

A. A 3-D Deterministic Simulation Model

This subsection proposes a SoS-based deterministic simulation model for HAP-MIMO channels and derives the corresponding channel impulse response and the STCF for a 3-D non-isotropic scattering environment.

Since the location of each scatterer inside the cylinder can be fully described by $a_R^{(n)}$, $R_S^{(n)}$, and $H_S^{(n)}$, the entire scattering region is considered as a 3-D point lattice partitioned into three scattering sub-regions, which are individually associated with one of these random variables. In particular, it is considered that N_1 scattering points are non-uniformly placed around a ring, N_2 scattering points are non-uniformly placed along a radial line, and N_3 scattering points are non-uniformly placed along a vertical line. Then, $N = N_1 N_2 N_3$ is the total finite number of discrete local scatterers, a random scatterer is now designated by $S^{(n_1,n_2,n_3)}$ and its location is controlled by $a_R^{(n_1)}$, $R_S^{(n_2)}$, and $H_S^{(n_3)}$, where $n_1 \in \{1,...,N_1\}$, $n_2 \in \{1,...,N_2\}$, and $n_3 \in \{1,...,N_3\}$.

Under these considerations and based on [17], the impulse response of the sub-channel *p-l* can be written as

$$\tilde{h}_{pl}(t) = \sqrt{\frac{K_{pl}}{K_{pl}+1}} h_{pl,LoS}(t) + \sqrt{\frac{1}{K_{pl}+1}} \tilde{h}_{pl,NLoS}(t), \quad (29)$$

where

$$\tilde{h}_{pl,NLoS}(t) = \frac{1}{\sqrt{N_1 N_2 N_3}} \sum_{n_1=1}^{N_1} \sum_{n_2=1}^{N_2} \sum_{n_3=1}^{N_3} e^{j\varphi^{(n_1,n_2,n_3)}}$$
$$\times e^{j2\pi t f_{R,\max} \cos\left(a_R^{(n_1)} - \gamma_R\right) \cos\left[\arctan\left(H_S^{(n_3)}/R_S^{(n_2)}\right)\right]}$$
$$\times e^{-j\frac{2\pi}{\lambda}\left(d'_{T,NLoS} + d'_{R,NLoS}\right)} \quad (30)$$

is the NLoS component of the impulse response, $h_{pl,LoS}(t)$ is defined in (2) “ $\tilde{\cdot}$ ” describes a deterministic time averaged quantity, and $d'_{T,NLoS}$ and $d'_{R,NLoS}$ are expressed, respectively, as

$$d'_{T,NLoS} \approx \frac{D}{\cos\beta_T} - \frac{0.5(n_T + 1 - 2p)\delta_T \cos\theta_T \cos\psi_T}{\cos\beta_T}$$
$$- \frac{0.5(n_T + 1 - 2p)\delta_T \sin\theta_T \cos\psi_T R_S^{(n_2)} \sin a_R^{(n_1)}}{D\cos\beta_T}, \quad (31)$$

$$d'_{R,NLoS} \approx R^{(n_2)} / \cos\left[\arctan\left(H_S^{(n_3)} / R_S^{(n_2)}\right)\right]$$
$$-0.5(n_R + 1 - 2l)\delta_R \cos\psi_R \cos\left(\theta_R - \alpha_R^{(n_1)}\right)$$
$$\times \cos\left[\arctan\left(H_S^{(n_3)} / R_S^{(n_2)}\right)\right] - 0.5(n_R + 1 - 2l)\delta_R \sin\psi_R$$
$$\times \sin\left[\arctan\left(H_S^{(n_3)} / R_S^{(n_2)}\right)\right]. \quad (32)$$

Providing that a sufficient large number of scatterers is used, i.e., $N = N_1 N_2 N_3 \geq 20$, central limit theorem implies that $\tilde{h}_{pl,NLoS}(t)$ is close to a low-pass zero-mean complex Gaussian process.

The STCF between two arbitrary subchannels $\tilde{h}_{pl,NLoS}(t)$ and $\tilde{h}_{qm,NLoS}(t)$ is defined as

$$\tilde{R}_{pl,qm}^{NLoS}(\delta_T, \delta_R, \tau) = \mathrm{E}\left[\tilde{h}_{pl,NLoS}(t) \tilde{h}_{qm,NLoS}^{*}(t+\tau)\right]$$
$$\approx \frac{(N_1 N_2 N_3)^{-1}}{\sqrt{(K_{pl}+1)(K_{qm}+1)}} \sum_{n_1=1}^{N_1} \sum_{n_2=1}^{N_2} \sum_{n_3=1}^{N_3} e^{j\frac{2\pi(q-p)\delta_T \cos\theta_T \cos\psi_T}{\lambda\cos\beta_T}}$$
$$\times e^{\frac{j2\pi(q-p)\delta_T \sin\theta_T \cos\psi_T R_S^{(n_2)} \sin a_R^{(n_1)}}{\lambda D \cos\beta_T}}$$
$$\times e^{\frac{j2\pi(m-l)\delta_R \sin\psi_R \sin\left[\arctan\left(H_S^{(n_3)}/R_S^{(n_2)}\right)\right]}{\lambda}}$$
$$\times e^{\frac{j2\pi(m-l)\delta_R \cos\theta_R \cos\psi_R \cos a_R^{(n_1)} \cos\left[\arctan\left(H_S^{(n_3)}/R_S^{(n_2)}\right)\right]}{\lambda}}$$
$$\times e^{\frac{j2\pi(m-l)\delta_R \sin\theta_R \cos\psi_R \sin a_R^{(n_1)} \cos\left[\arctan\left(H_S^{(n_3)}/R_S^{(n_2)}\right)\right]}{\lambda}}$$
$$\times e^{-j2\pi\tau f_{R,\max} \cos\left(a_R^{(n_1)} - \gamma_R\right) \cos\left[\arctan\left(H_S^{(n_3)}/R_S^{(n_2)}\right)\right]}. \quad (33)$$

From (33), it is obvious that $a_R^{(n_1)}$, $R_S^{(n_2)}$, and $H_S^{(n_3)}$ must be properly determined, such that the simulation model approximates the reference model. Note that no parameter computation method will be applied to the phases $\varphi^{(n_1,n_2,n_3)}$, since the STCF does not depend on them. Notwithstanding, the interest reader is referred to [28], where an efficient method to compute the phases is given. Following a similar approach to that proposed in [17], the aforementioned parameters are generated as follows

$$a_R^{(n_1)} = F_{a_R}^{-1}\left(\frac{n_1 - 0.5}{N_1}\right), \quad (34)$$

$$R_S^{(n_2)} = F_{R_S}^{-1}\left(\frac{n_2 - 0.5}{N_2}\right), \quad (35)$$

$$H_S^{(n_3)} = F_{H_S}^{-1}\left(\frac{n_3 - 0.5}{N_3}\right) \quad (36)$$

for $n_1 = 1,...,N_1$, $n_2 = 1,...,N_2$, and $n_3 = 1,...,N_3$. Hence, the proposed deterministic model computes constant values for the model parameters, needs a single run to obtain the desired statistical properties and hence has short simulation times. However, it is important to properly determine the number of scattering points, i.e., N_1, N_2, and N_3, needed to achieve a desired convergence level. Indeed, the complexity of the deterministic simulation model is controlled by N_1, N_2, and N_3. Thus, N_1, N_2, and N_3 should be carefully determined to reduce the computation load of the complete channel simulator and improve the efficiency and the reliability of the proposed model.

The MIMO channel models are generally classified into physical or non-physical (analytical) models based on the modeling philosophy [29]. Physical channel models depend on the characteristics of the propagation environment and allow for an accurate reproduction of the real channel. On the contrary, non-physical models synthesize the MIMO channel matrix in the context of system and algorithm development and verification and can be further subdivided into propagation-motivated models and correlation-based models.

Due to the different way of generation of $\mathbf{H}_{NLoS}$, the reference model is referred to as the non-physical model, while the deterministic model is referred to as the physical model. In particular, the reference model generates the elements of $\mathbf{H}_{NLoS}$ using (11)-(14), (19) and (20). On the contrary, the deterministic model generates the elements of $\mathbf{H}_{NLoS}$ using (30) and hence $\mathbf{H}_{NLoS}$ is given by

$$\mathbf{H}_{NLoS} = \begin{bmatrix} \tilde{h}_{11,NLoS} & \cdots & \tilde{h}_{1n_T,NLoS} \\ \vdots & \ddots & \vdots \\ \tilde{h}_{n_R 1,NLoS} & \cdots & \tilde{h}_{n_R n_T,NLoS} \end{bmatrix}. \qquad (37)$$

B. Simulation Results

In this section, the performance of the deterministic simulation model is evaluated. The values of the model parameters used are $\mathrm{SNR} = 15$ dB, $K_{pl} = K_{qm} = K = 3$ dB, $H_T = 20$ km, $\beta_T = 60^\circ$, $\delta_T = 50\lambda$, $\delta_R = 0.5\lambda$, $\theta_T = 60^\circ$, $\theta_R = 30^\circ$, $\psi_T = 0^\circ$, $\psi_R = 30^\circ$, $k = 5$, $\mu = 60^\circ$, $a = 0.01$, $R_{S,\max} = 180$ m, $H_{S,\max} = 70$ m, $H_{S,\text{mean}} = 17.6$ m, $\sigma = 0.31$, $f_{R,\max} = 100$ Hz, $\gamma_R = 30^\circ$, $N_1 = 30$, $N_2 = 20$, and $N_3 = 5$. Finally, a normalized sampling period $f_{R,\max} T_s = 0.02$ is used, where T_s is the sampling period.

The goal of any simulation model is to reproduce the channel's desired statistical properties. Figures 12 and 13 investigate the performance of the deterministic model for different complexity, i.e., different N_1, N_2, and N_3, in terms of the temporal correlation function (TCF), i.e., $n_T = n_R = 1$, for the time delay range $0 \text{ s} \le \tau \le 0.1 \text{ s}$, which is typically of interest for many communications systems, and the spatial correlation function (SCF), i.e., $\tau = 0$, for the ranges $0 \le \delta_T \le 200\lambda$ and $0 \le \delta_R \le 3\lambda$, respectively. As soon as the value of the Ricean factor is sufficiently small, the maximum values of the range of the inter-element distances chosen, i.e., 200λ and 3λ, ensure low spatial correlation in many propagation scenarios, as shown in [2]. The effect of the variation of each number of coordinates of scattering points is examined independently, provided that the other numbers are sufficiently large and do not affect the simulation results. The performance evaluation is realized in terms of the root mean square error (RMSE) between the absolute TCFs and SCFs of the simulation model and the reference model. According to Figures 12 and 13, the performance can be improved by increasing the number of the discrete local scatterers, i.e., N_1, N_2, and N_3, and thus the complexity of the proposed model. Figures 12 and 13 also suggest that reasonable values for N_1 (associated with a_R), N_2 (associated with R_S), and N_3 (associated with H_S) are in the order of 30, 20, and 5, respectively.

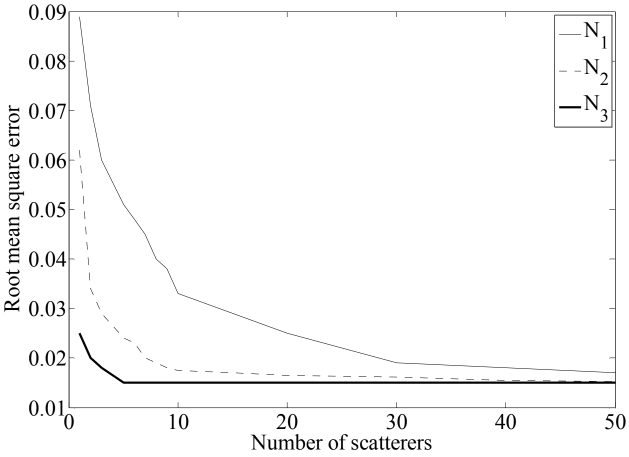

Figure 12. Performance evaluation of the deterministic simulation model in terms of the temporal correlation function.

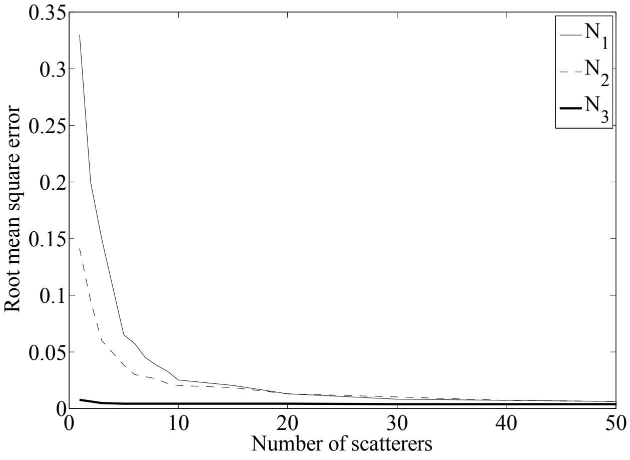

Figure 13. Performance evaluation of the deterministic simulation model in terms of the spatial correlation function.

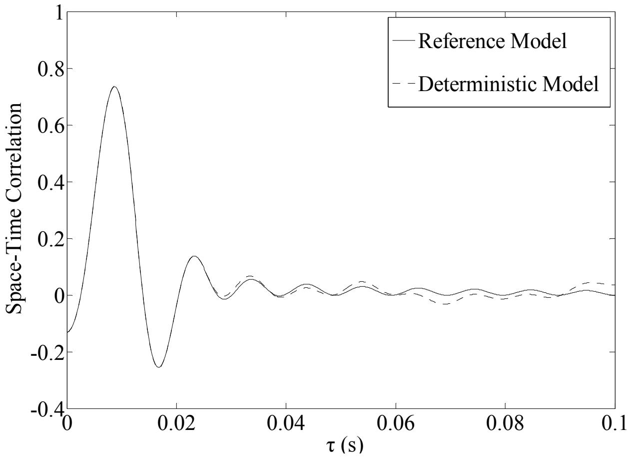

Figure 14. Real part of the STCFs of the NLoS component of the reference model and the deterministic model.

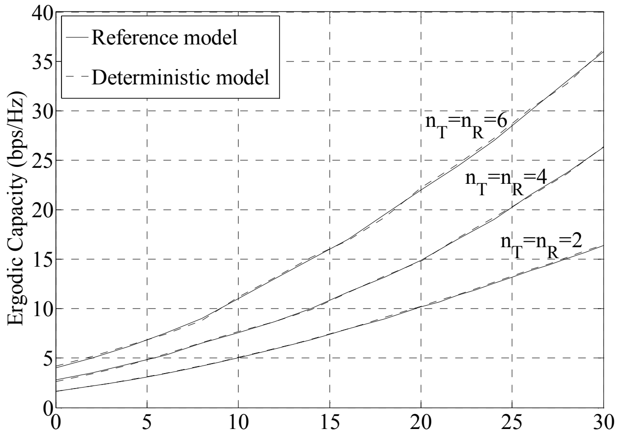

Figure 15. Comparison between the ergodic capacities obtained using the reference and the deterministic model for different number of antenna elements.

Figure 14 compares the real part of the STCFs of the NLoS component associated with the reference and the simulation model. One observes that the STCF of the deterministic model closely matches the reference one for the time delay range $0 \le \tau(\mathrm{s}) \le 0.1$. We also obtain that the RMSE between the absolute STCFs of the deterministic model and the reference model is 0.026 for $N_1 = 30$, $N_2 = 20$, and $N_3 = 5$, and 0.018 for $N_1 = 40$, $N_2 = 30$, and $N_3 = 10$. Hence, increasing the number of scatterers, enhances the performance of the deterministic model.

Finally, Figure 15 compares the ergodic capacity against SNR for different number of antenna elements ($n_T = n_R = 2$, $n_T = n_R = 4$, and $n_T = n_R = 6$) obtained using the reference and the deterministic models. The results show very good agreement between the non-physical and the physical models and verify the usefulness of the proposed simulation model. These results also show that increasing the number of antenna elements, increases the prospective MIMO capacity gain. Nevertheless, when multiple antenna elements are utilized, these antenna elements should be placed at significant distances from each other to ensure that the paths are really diverse. Hence, the HAP length should be adequate to accommodate two or more antenna elements.

VI. CONCLUSION AND FUTURE WORK

In this paper, the channel capacity of a HAP-based communications system equipped with multi-element antennas at both sides has been defined and investigated. Specifically, the capacity has been studied taking into account a recently proposed 3-D reference model for HAP-MIMO channels. The numerical results have demonstrated that the MIMO architecture outperforms the conventional SISO architecture in terms of the channel capacity. These results have also shown that the capacity depends on the strength of the LoS signal and the received SNR. Specifically, increasing the Ricean factor decreases the capacity, while increasing the SNR and the number of antenna elements increases the capacity. Furthermore, the results have underlined the effects of spatial and temporal correlation on the capacity of ULAs and have suggested that applying MIMO techniques to a single HAP can effectively enhance the capacity, as soon as the Ricean factor is small. In particular, the influence of the elevation angle of the platform, the antenna configuration and displacement, the mobility of the terrestrial station, and the non-uniform distribution of the local scatterers on the capacity has been analyzed. It has been shown that increasing the elevation angle of the platform increases the capacity, while increasing the density of the scatterers in the vicinity of the user and the spacing between the antennas increases the capacity. Moreover, broadside HAP antennas maximize the capacity, while vertically placed antennas at the mobile terminal provide considerable capacity gain in highly urbanized areas. Finally, the results have underlined that changing the velocity and the moving direction of the user significantly affects the capacity. From the non-realizable reference model, a 3-D deterministic simulation model for HAP-MIMO mobile fading channels has been proposed. The simulation results have shown that the simulation model satisfactorily approximates the reference one in terms of the correlation properties and the channel capacity.

The capacity analysis and the proposed deterministic simulation model provide a convenient framework for the analysis, design, test, and optimization of future HAP-MIMO communications systems. Nevertheless, this work could be further improved or extended into different areas. Due to the lack of channel-sounding measurement campaigns, the contribution of this work has been limited to developing a simulation model for HAP-MIMO channels. However, it is important to verify the theoretical model in real-world propagation conditions. Specifically, HAPs could be emulated by using a helicopter, a small plane or a balloon containing two or more antennas sufficiently separated. However, access to a real HAP would be even more ideal. In addition, the analysis in this paper is restricted to HAP-MIMO systems employing ULAs at both sides of the communication link. The HAP-MIMO channel models can be modified to employ other antenna array geometries, such as uniform planar arrays (UPAs), uniform circular arrays (UCAs), and spherical antenna arrays (SAAs), or a combination of them. Apart from considering only single-bounce rays, this work can also be extended to additionally support double-bounce or multiple-bounce rays (due to multiple scattering, reflection or diffraction of the radiated energy). Then, more sophisticated and realistic channel models can be obtained. Finally, there is perhaps an opportunity to extend the material in the paper by taking into account the energy efficiency issues, i.e., investigating the impact of possible power constraints at the wireless devices on the available channel capacity of HAP-MIMO channels.

REFERENCES

[1] E. T. Michailidis and A. G. Kanatas, "On the Capacity of 3-D Space-Time Correlated HAP-MIMO Channels," in *Proc. 2nd International Conference on Advances in Satellite and Space Communications (SPACOMM) 2010*, Athens/Glyfada, Greece, pp. 87-92, 13-19 Jun. 2010.

[2] E. T. Michailidis and A. G. Kanatas, "Three Dimensional HAP-MIMO Channels: Modeling and Analysis of Space-Time Correlation," *IEEE Transactions on Vehicular Technology*, vol. 59, no. 5, pp. 2232-2242, Jun. 2010.

[3] A. Aragón-Zavala, J. L. Cuevas-Ruíz, and J. A. Delgado-Penín, *High-Altitude Platforms for Wireless Communications*, New York, USA: John Wiley & Sons, Dec. 2008.

[4] S. Karapantazis and F. Pavlidou, "Broadband communications via high-altitude platforms: A survey," *IEEE Communications Society Surveys & Tutorials*, vol. 7, no. 1, pp. 2-31, 2005.

[5] A. K. Widiawan and R. Tafazolli, "High Altitude Platform Station (HAPS): A Review of New Infrastructure Development for Future Wireless Communications," *Wireless Personal Communications*, vol. 42, no. 3, pp. 387-404, Aug. 2007.

[6] A. Mohammed and Z. Yang, "Broadband Communications and Applications from High Altitude Platforms," *International Journal of Recent Trends in Engineering*, vol. 1, no. 3, pp. 239-243, May 2009.

[7] "Minimum performance characteristics and operational conditions for high altitude platform stations providing IMT-2000 in the bands 1885–1980 MHz, 2010–2025 MHz and 2110–2170 MHz in region 1 and 3 and 1885–1980 MHz and 2110–2160 MHz in region 2," *International Telecommunication Union*, Geneva, Switzerland, ITU-R Recommendation F.1456, 2000.

[8] A. Paulraj, R. Nabar, and D. Gore, *Introduction to Space-Time Wireless Communications*, Cambridge, UK: Cambridge University Press, 2003.

[9] E. Telatar, "Capacity of multi-antenna Gaussian channels," *European Transactions on Telecommunications*, vol. 10, no. 6, pp. 585-595, 1999.

[10] G. J. Foschini and M. J. Gans, "On Limits of Wireless Communications in a Fading Environment when Using Multiple Antennas," *Wireless Personal Communications*, vol. 6, no. 3, pp. 311-335, 1998.

[11] P.-D. Arapoglou, E. T. Michailidis, A. D. Panagopoulos, A. G. Kanatas, and R. Prieto-Cerdeira, "The Land Mobile Earth-Space Channel: SISO to MIMO Modeling from L- to Ka-Bands," *IEEE Vehicular Technology Magazine, Special Issue on Trends in Mobile Radio Channels: Modeling, Analysis, and Simulation*, vol. 6, no. 2, pp. 44-53, Jun. 2011.

[12] D. I. Axiotis, M. E. Theologou, and E. D. Sykas, "The effect of platform instability on the system level performance of HAPS UMTS," *IEEE Communications Letters*, vol. 8, no. 2, pp. 111-113, Feb. 2004.

[13] K. Katzis, D. A. J. Pearce, and D. Grace, "Impact of high altitude platform movements on cellular handover," in *Proc. International Workshop on High Altitude Platform Systems*, Athens, Greece, Sep. 2005.

[14] S. O. Rice, "Mathematical analysis of random noise," *Bell Systems Technical Journal*, vol. 23, pp. 282-332, Jul. 1944.

[15] C. Xiao, Y. R. Zheng, and N. C. Beaulieu, "Novel sum-of-sinusoids simulation models for Rayleigh and Rician fading channels," *IEEE Transactions on Wireless Communications*, vol. 5, no. 12, pp. 3667-3679, Dec. 2006.

[16] C.-X. Wang, M. Patzold, and D. Yuan, "Accurate and efficient simulation of multiple uncorrelated Rayleigh fading waveforms," *IEEE Transactions on Wireless Communications*, vol.6, no.3, pp.833-839, Mar. 2007.

[17] A. G. Zajić, and G. L. Stüber, "Three-dimensional modeling, simulation, and capacity analysis of space-time correlated mobile-to-mobile channels," *IEEE Transactions on Vehicular Technology*, vol. 57, no. 4, pp. 2042-2054, Jul. 2008.

[18] A. Abdi and M. Kaveh, "A space-time correlation model for multielement antenna systems in mobile fading channels," *IEEE Journal on Selected Areas in Communications,* vol. 20, no. 3, pp. 550-560, Apr. 2002.

[19] A. Abdi, J. A. Barger, and M. Kaveh, "A parametric model for the distribution of the angle of arrival and the associated correlation function and power spectrum at the mobile station," *IEEE Transactions on Vehicular Technology*, vol. 51, no. 3, pp. 425-434, May 2002.

[20] S. S. Mahmoud, Z. M. Hussain, and P. O'Shea, "Space-time model for mobile radio channel with hyperbolically distributed scatterers," *IEEE Antennas and Wireless Propagation Letters*, vol. 1, pp. 211-214.

[21] S. S. Mahmoud, Z. M. Hussain, and P. O'Shea, "A geometrical-based microcell mobile radio channel model," *Wireless Networks*, vol. 12, no. 5, pp. 653-664, Sep. 2006.

[22] M. A. Vázquez-Castro, F. Perez-Fontan, and S. R. Saunders, "Shadowing correlation assessment and modeling for satellite diversity in urban environments," *International Journal of Satellite Communications*, vol. 20, no. 2, , pp. 151-166, March/April 2002.

[23] C. Tzaras, B. G. Evans, and S. R. Saunders, "Physical-statistical analysis of land mobile-satellite channel," *Electronics Letters*, vol. 34, no. 13, pp. 1355-1357, Jun. 1998.

[24] I. S. Gradshteyn and I. M. Ryzhik, *Table of Integrals, Series and Products*, 5th edition, Edited by A. Jeffrey, Academic Press, 1994.

[25] D.-S. Shiu, G. J. Foschini, M. J. Gans, and J. M. Kahn, "Fading correlation and its effect on the capacity of multielement antenna systems," *IEEE Transactions on Communications*, vol. 48, no. 3, pp. 502-513, Mar. 2000.

[26] R. U. Nabar, Ö. Oyman, H. Bolcskei, and A. J. Paulraj, "Capacity scaling laws in MIMO wireless networks," in *Proc. 41st Allerton Conference on Communication, Control, and Computing 2003*, pp. 378-389, Monticello-Illinois, USA, Oct. 2003.

[27] K. V. Mardia and P. E. Jupp, *Directional Statistics*, New York: Wiley, 1999.

[28] M. Pätzold, U. Killat, F. Laue, and Y. Li, "On the properties of deterministic simulation models for mobile fading channels," *IEEE Transactions on Vehicular Technology*, vol. 47, no. 1, pp. 254-269, Feb. 1998.

[29] P. Almers, E. Bonek, A. Burr, et al., "Survey of Channel and Radio Propagation Models for Wireless MIMO Systems," *EURASIP Journal on Wireless Communications and Networking*, vol. 2007, 2007.